A Method of Tracking Optimum Efficiency for Four-Coil Wireless Power Transfer System

Zhongqi Li*, **Yixiong Lai, Jiliang Yi, and Junjun Li**

Abstract—Magnetic resonant wireless power transfer (WPT) is an emerging technology that may create new applications for wireless power charging. However, low efficiency resulting from the change of the transfer distance is a main obstructing factor for promoting this technology. In this paper, a method of fast tracking optimum efficiency is proposed. The input impedance value is obtained by measuring the input current. Then the transfer distance is estimated by the input impedance value. The optimum load resistor is obtained under a given transfer distance. In addition, the extended L-matching network is proposed in order to automatically adjust the load resistor. The key parameters of the matching network are also given. The optimum efficiency can be fast tracked by the proposed method as the transfer distance varies. The WPT system and the extended L-matching network are designed. Simulated and experimental results validating the proposed method are given.

1. INTRODUCTION

Wireless power transfer (WPT) methods are receiving increasing attention in the international research community. A new wireless power transfer technology based on strongly coupled magnetic resonances is proposed [1–5]. This technology is used widely in the fields of medical devices, charging of mobile and electric vehicles due to its high efficiency [6–9].

The transfer efficiency is high when the WPT system operates in the critically-coupled regime [8], whereas the transfer efficiency is low at the original resonant frequency when the system operates in the over-coupled or under-coupled regimes [10]. The system may be transformed from the critically-coupled regime to the over-coupled or under-coupled regimes as the transfer distance is changed. There are three methods to improve the system efficiency. The first method is to adjust the operating frequency [10–12]. The second method is to adjust the coupling coefficients between the source coil and transmission coil, and between the receiving coil and load coil [13]. The third method is to adjust the load resistor [14]. However, the first method is only suitable for the system operating in the over-coupled regime. The second method is difficult to implement, because it requires mechanically adjusting the distance between coils. And it is well known that the load resistor is nearly constant for a given load.

In order to adjust the equivalent load resistor, there are several types of impedance matching networks such as the L-match, Pi-match and DC-DC match networks. A novel cascaded boost-buck DC-DC converter is proposed. The equivalent load resistor can be changed by adjusting the duty cycle of DC-DC converter [15]. The L-match impedance matching network is proposed [16]. The equivalent load resistor can also be changed by adjusting the values of capacitors. However, the feedback control mechanism is not introduced in the previous methods adjusting the equivalent load resistor. Therefore, the system is only suitable for the situation of fixed transfer distance. In order to automatically track the maximum efficiency for varied transfer distance, a maximum efficiency point tracking control scheme is proposed. Double DC-DC converters are used, the transmission side dc/dc converter is used to adjust the input voltage conversion ratio, and the receiving side dc/dc converter is used to adjust the load resistor

conversion ratio. The optimum load resistor conversion ratio can be obtained by continuous changing duty cycle of DC-DC converter [17]. A method for automatic "maximum energy efficiency tracking" operation for wireless power transfer systems is presented. The minimum input power operating point is tracked by real-time changing the duty cycle of Buck-Boost converter [18]. Changing the duty cycle of DC-DC converter is to satisfy the impedance matching. However, when the transfer distance varies, the system need to continuously search the optimum duty cycle of DC-DC converter as the maximum efficiency tracking methods in [17, 18] are used. If the transfer distance varies fast, the search steps should be minimized to real-time track the maximum efficiency point. A novel serial/parallel capacitor matrix in the transmitter is presented to track automatically the optimum impedance-matching point when the transfer distance varies [19]. Moreover, a window-prediction based search algorithm is presented in order to decrease the search steps.

In order to minimize the search steps and track the optimum efficiency, a fast tracking optimum efficiency (FTOE) method is proposed in this paper. The input impedance value is obtained by measuring the input current. Then the transfer distance is estimated by the input impedance value. The optimum load resistor is obtained under a given transfer distance. The optimum efficiency can be achieved by adjusting the equivalent load resistor. And the impedance network is used to automatically adjust the equivalent load resistor. The significant characteristic is that the proposed method can fast track the optimum efficiency. In this paper, we investigate how the optimum efficiency is fast tracked when the transfer distance varies. The load resistor is fixed at $50\,\Omega$ and the load resistor variation is out of my scope.

The rest of the paper is organized as follows. Section 2 establishes the system model and theory. Section 3 analyzes the FTOE method. Section 4 presents the simulation results. Section 5 presents the experimental setup and the measurement results. Section 6 concludes this paper.

2. MODEL AND THEORETICAL ANALYSIS

The WPT system is composed of four resonant coils: source, transmission, receiving and load resonant coils, labeled as S, Tx, Rx and L resonant coils, as shown in Fig. 1. All the resonant coils are assumed to be aligned coaxially. D is the distance between Tx and Rx resonant coils. The WPT system can be represented in terms of lumped circuit elements (L_m, C_m, and R_m ($m = 1\,(\mathrm{S})$, $2\,(\mathrm{Tx})$, $3\,(\mathrm{Rx})$, $4\,(\mathrm{L})$)), as shown in Fig. 2. L_m is the self-inductance of each coil, C_m the compensation capacitor of each coil, R_m the parasitic resistance of each coil, V_s the source power, R_s the internal resistor of power, R_L the load resistor, R_L equal to $50\,\Omega$, and k_{mn} the coupling coefficient between m and n resonant coils. The cross-coupling coefficients are very small, and they can be neglected in the following analysis. ω is the operating angular frequency, ω_m the resonant angular frequency of each coil, ω_0 the original resonant angular frequency, and Z_{in} the input impedance.
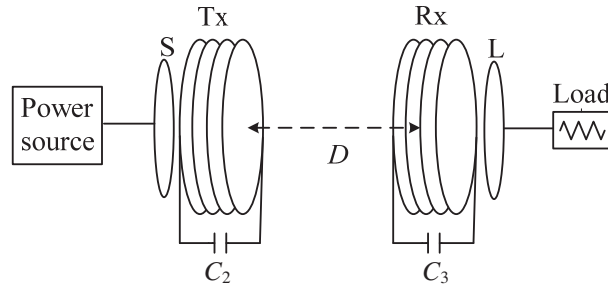
Figure 1. The simplified schematic of the WPT system based on magnetically coupling resonator.

By applying Kirchhoff's voltage law (KVL), the WPT system is presented as follows [10]:

$$\begin{cases} Z_1 I_1 + j\omega M_{12} I_2 = V_s \\ j\omega M_{12} I_1 + Z_2 I_2 + j\omega M_{23} I_3 = 0 \\ j\omega M_{23} I_2 + Z_3 I_3 + j\omega M_{34} I_4 = 0 \\ j\omega M_{34} I_3 + Z_4 I_4 = 0 \end{cases} \tag{1}$$
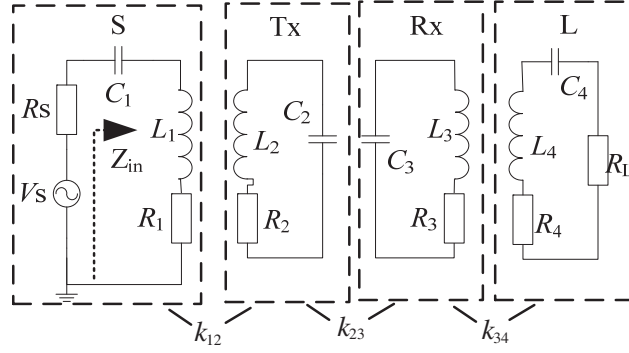
Figure 2. The equivalent circuit model for the WPT system. Each coil is modeled as series resonators.

$$\begin{cases} Z_1 = R_1 + R_s + j\omega L_1 + 1/(j\omega C_1) \\ Z_2 = R_2 + j\omega L_2 + 1/(j\omega C_2) \\ Z_3 = R_3 + j\omega L_3 + 1/(j\omega C_3) \\ Z_4 = R_4 + R_L + j\omega L_4 + 1/(j\omega C_4) \end{cases} \tag{2}$$

where I_m is the current of each coil, and M_{mn} is the mutual inductance between m and n resonant coils. According to Eqs. (1) and (2), the efficiency expression is obtained as follows:

$$\eta = \frac{I_4^2 R_L}{V_s I_1} = \frac{\omega^9 k_{12}^2 k_{23}^2 k_{34}^2 Q_L}{\begin{aligned} &64\omega^2(Q_1+Q_s)(A^2+B^2)+4Q_2\omega^2 k_{12}^2\{[-32\delta^2+8\omega^2 k_{34}^2+4Q_3(Q_4+Q_L)]^2 \\ &+[8(Q_4+Q_L)\delta+8Q_3\delta]^2\}+Q_3[4\omega^6 k_{12}^2 k_{23}^2\delta^2+\omega^6 k_{12}^2 k_{23}^2(Q_4+Q_L)^2] \\ &+\omega^9 k_{12}^2 k_{23}^2 k_{34}^2(Q_4+Q_L) \end{aligned}} \tag{3}$$

where

$$A = Q_2 Q_3 \delta/4\omega^2 + (Q_2+Q_3)(Q_4+Q_L)\delta/4\omega^2 - \delta^3 + \omega^2 k_{34}^2 \delta/4 + \omega^2 k_{23}^2 \delta/4$$

$$B = Q_2 Q_3 (Q_4+Q_L)/8\omega^3 - (Q_2+Q_3+Q_4+Q_L)\delta^2/2\omega + \omega Q_2 k_{34}^2/8 + \omega(Q_4+Q_L)k_{23}^2/8$$

I_1 is the input current. The angular frequency deviation factor is defined as $\delta = \omega_0 - \omega$, the unload quality factor of the S coil defined as $Q_1 = \omega L_1/R_1$, the unload quality factor of the Tx coil defined as $Q_2 = \omega L_2/R_2$, the unload quality factor of the Rx coil defined as $Q_3 = \omega L_3/R_3$, the unload quality factor of the L coil defined as $Q_4 = \omega L_4/R_4$, the quality factor of power source defined as $Q_S = \omega L_1/R_s$, and the quality factor of load defined as $Q_L = \omega L_4/R_L$.

Assuming $\omega_1 = \omega_2 = \omega_3 = \omega_4 = \omega_0$, the efficiency expression (3) can be simplified as follows:

$$\eta = \frac{U_L U_1^2 U_2^2 U_3^2}{\left\{(1+U_s)\left[(1+U_L)+U_3^2+U_2^2(1+U_L)\right]^2+U_1^2\left[(1+U_L)+U_3^2\right]^2+(1+U_L)^2 U_1^2 U_2^2+(1+U_L)^2 U_1^2 U_2^2 U_3^2\right\}} \tag{4}$$

where the source matching factor is defined as $U_s = R_s/R_1$, the load matching factor defined as $U_L = R_L/R_4$, the strong-coupling parameter between S and Tx defined as $U_1 = k_{12}^2 Q_1 Q_2$, the strong-coupling parameter between Tx and Rx defined as $U_2 = k_{23}^2 Q_2 Q_3$, and the strong-coupling parameter between Rx and L defined as $U_3 = k_{34}^2 Q_3 Q_4$.

By differentiating η with respect to U_L and equating the differential function to zero

$$\frac{\partial \eta}{\partial U_L} = 0 \tag{5}$$

The load matching factor for the optimum efficiency can be obtained as follows:

$$U_{L\_opt} = \frac{\begin{aligned} &[(U_s U_2^2+2U_s U_2+U_2^2+U_s+1+U_1 U_2+2U_2)(U_s+1+2U_s U_1+2U_s U_2 \\ &+2U_s U_1 U_2+3U_2^2+U_1^2 U_2+3U_1+2U_2+U_2^2+U_s U_2^2+3U_1 U_2+U_s U_1^2+U_1^3)]^{1/2} \end{aligned}}{1+2U_s U_2+2U_2+U_s+U_1+U_2^2+U_1 U_2+U_s U_2^2} \tag{6}$$

In order to obtain the optimum efficiency, the optimum load resistor R_{L_opt} (influencing U_{L_opt} in Eq. (6), $U_{L\_opt} = R_{L\_opt}/R_4$) should be satisfied.

3. NEW METHOD FOR FTOE

In this section, a fast tracking optimum efficiency method is illustrated with the help of the circuit structure in Fig. 3. The input impedance values Z_{in} can be obtained by measuring the input voltage and input current. M_{23} value can be calculated by Z_{in} value according to (13). For a given M_{23}, the optimum load resistor R_{L_opt} can be obtained according to Eq. (6). The equivalent load resistor can be adjusted by the L-type matching network. C_s and C_p values in the L-type matching network can be obtained according to R_{L_opt}.
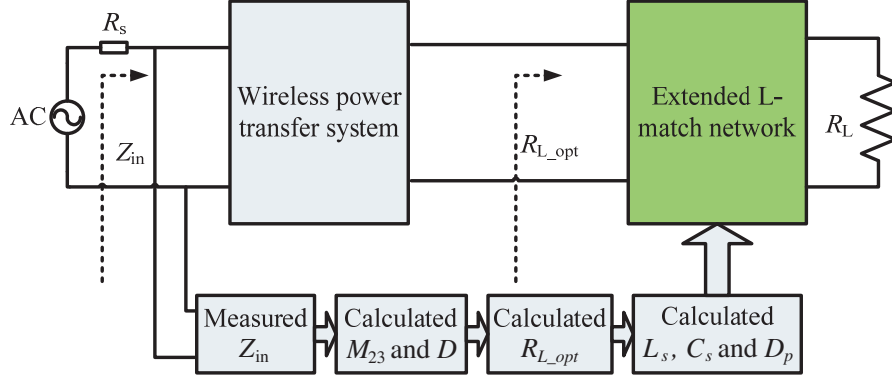
Figure 3. The circuit structure of the FTOE method.

3.1. Estimation of the Transfer Distance D

The transfer distance **D** can be represented by the mutual impedance M_{23} between Tx and Rx. If M_{23} value may be obtained, the transfer distance may be estimated.

The mutual inductance of two coaxial circular current loops can be stated in terms of complete elliptic integrals [20]:

$$M = \mu_0 \frac{\sqrt{R_P R_S}}{b} \left[\left(2 - b^2\right) K(b) - 2E(b) \right] \tag{7}$$

where

$$b = \sqrt{\frac{4R_P R_S}{h^2 + (R_P + R_S)^2}} \tag{8}$$

$$K(b) = \int_0^{\pi/2} \frac{1}{\sqrt{1 - b^2 \sin^2 \theta}} d\theta \tag{9}$$

$$E(b) = \int_0^{\pi/2} \sqrt{1 - b^2 \sin^2 \theta} d\theta \tag{10}$$

M is the mutual inductance of two circular loops of radii R_P and R_S, h the distance between loops, $K(b)$ the complete elliptic integral of the first kind, and $E(b)$ the complete elliptic integral of the second kind. The relationship between the mutual inductance and the distance can be obtained from Eqs. (7)–(10).

M_{23} value may be obtained by the input impedance. The input impedance is defined as $Z_{\text{in}} = V_s/I_1 - R_s$, Z_{in} may then be obtained from Eqs. (1) and (2).

$$Z_{in} = \frac{\omega^4 M_{12}^2 M_{34}^2 + \omega^2 M_{12}^2 Z_3 Z_4 + \omega^2 M_{23}^2 Z_1 Z_4 + \omega^2 M_{34}^2 Z_1 Z_2 + Z_1 Z_2 Z_3 Z_4}{\omega^2 M_{23}^2 Z_4 + \omega^2 M_{34}^2 Z_2 + Z_2 Z_3 Z_4} - R_s \tag{11}$$

Assuming the system operates in the resonant state, Equation (2) can be simplified as follows:

$$\begin{cases} Z_1 = R_1 + R_s \\ Z_2 = R_2 \\ Z_3 = R_3 \\ Z_4 = R_4 + R_L \end{cases} \tag{12}$$

Equation (12) is substituted into Equation (11), and Equation (13) can be obtained as follows:

$$M_{23} = \sqrt{\frac{\begin{Bmatrix} \omega^4 M_{12}^2 M_{34}^2 + \omega^2 M_{12}^2 R_3(R_4 + R_L) + \omega^2 M_{23}^2(R_1 + R_s)(R_4 + R_L) \\ +\omega^2 M_{34}^2(R_1 + R_s)R_2 - (Z_{in} + R_s)[\omega^2 M_{34}^2 R_2 + R_2 R_3(R_4 + R_L)] \end{Bmatrix}}{(Z_{in} + R_s)\omega^2(R_4 + R_L) - \omega^2(R_1 + R_s)(R_4 + R_L)}} \tag{13}$$

Z_{in} value can be obtained by measuring the input current I_1. M_{23} value can be calculated from Eq. (13) when the parameters of the resonant coils and the load resistor are given. Then, the transfer distance D can be calculated from Eqs. (7)–(10). The optimum load resistor R_{L_opt} can be obtained according to Eq. (6) under a given transfer distance D.

3.2. Analysis of the L-Match Network

The impedance matching network is used to automatically change the equivalent load resistor. There are several types of impedance matching networks such as the L-match, Pi-match and DC-DC match networks. All matching networks can match the impedance of the WPT system. The L-match network is simple. Therefore, it is used in this paper. The L-match network includes the L-type and inverted L-type matching networks, as shown in Fig. 4.
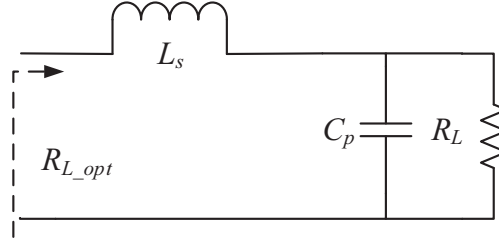
Figure 4. The circuits of the L-match network.

Figure 4 shows the L-type matching circuit. Using the circuit theory, its equivalent impedance equation can be obtained as follows:

$$R_{L-opt} = j\omega L_s + \frac{R_L}{1 + j\omega C_p R_L} \tag{14}$$

The imaginary and the real parts on both sides of Eq. (14) are equal. Equations (15) and (16) can be obtained according to Eq. (14).

$$C_p = \sqrt{\frac{(R_L/R_{L\_opt} - 1)}{\omega^2 R_L^2}} \tag{15}$$

$$L_s = \frac{C_p R_L^2}{1 + \omega^2 R_L^2 C_p^2} \tag{16}$$

C_p value can be obtained from Eq. (15) under a given R_{L_opt}. C_p value must be positive. Therefore, R_L value must be larger than R_{L_opt} value. The L-type matching network can be used when $R_L > R_{L\_opt}$. L_s value can be obtained from Eq. (16) under a given R_{L_opt}.

3.3. Design of the L-Match Network

The L-type matching network is used because R_L value ($R_L = 50\,\Omega$) is larger than R_{L_opt} value. R_{L_opt} is changed as the transfer distance is changed according to Eq. (6). C_p and L_s values are changed as R_{L_opt} is changed according to Eqs. (15) and (16). In order to automatically adjust R_{L_opt}, C_p and L_s values should be automatically adjusted. Two methods that use the capacitor matrix and inductance matrix are proposed to adjust C_p and L_s values, as shown in Fig. 5. Fig. 5(a) shows the extended L-match network using the inductance matrix, and the inductors are connected in serial according to

the switch array selection (S_{pm} and S_{sm}, $m = 1$–8). Fig. 5(b) shows the extended L-match network of using the capacitor matrix, and the capacitors are connected in parallel according to the switch array selection. The capacitor matrix is used in this paper because it is relatively easy to implement.

When switch S_1 is on, and switch S_2 is off, the extended L-match network is bypassed. The transfer
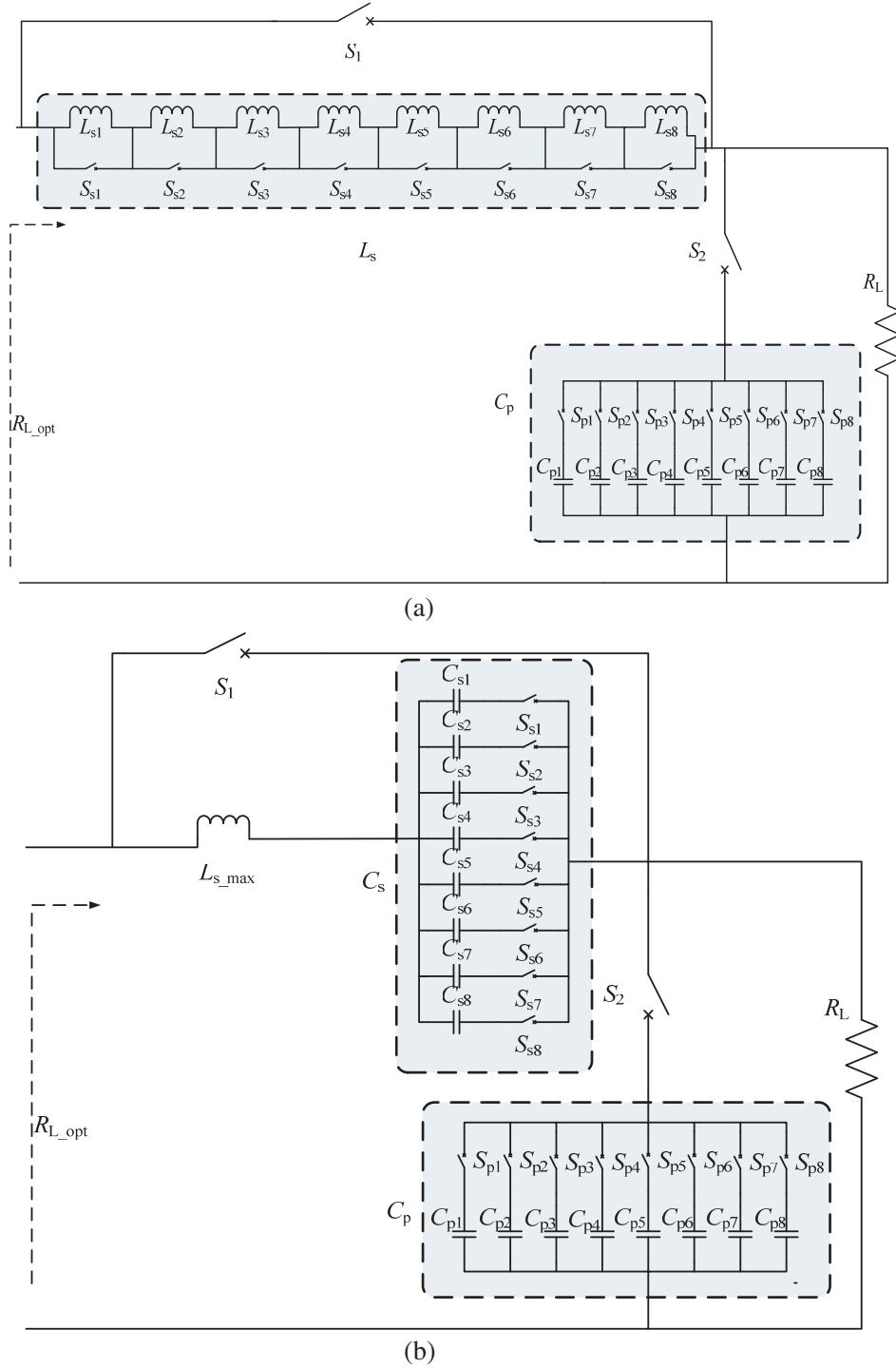
Figure 5. The extended L-match network. (a) The extended L-match network with using inductance matrix. (b) The extended L-match network with using capacitor matrix.

distance can be estimated from the previous analysis. The optimum load resistor R_{L_opt} can be obtained for different transfer distances. Then, C_p and L_s values are obtained from Eqs. (15) and (16) under a given R_{L_opt}. Table 1 shows C_p and L_s values when D is ranged from 15 cm to 40 cm. In order to adjust L_s value, the capacitor matrix (C_s) is connected to L_s in serial. The maximum L_s value is 26.22 µH from Table 1. The allowance of L_s is 20% of the maximum L_s. Therefore, L_{s_max} value is set at 30 µH. C_s value can be obtained according to Eq. (17).

$$C_s = \frac{1}{\omega^2(L_{s\_max} - L_s)} \tag{17}$$

C_s values are shown in Table 2 for different D. C_{sm} value is set at $3 \times 2^{m-1}$ nF ($m = 1$–8) in order to obtain different C_s values. C_{pm} value is set at $1 \times 2^{m-1}$ nF ($m = 1$–8) in order to obtain different C_p values. When the switch S_1 is off, and the switch S_2 is on, the L-type matching network is added into the WPT system to change the equivalent load resistor. If the measured input impedance value is changed, switch S_1 is on, and switch S_2 is off. Then the system restarts to estimate the transfer distance (the mutual inductance between Tx and Rx). Once the transfer distance is obtained, the system starts to rematch the equivalent load resistor by adjusting C_s and C_p values.

Table 1. C_p and L_s values for different D.

D/cm	C_p/nF	L_s/µH
15	194.82	12.66
20	160.15	15.21
25	133.22	17.98
30	112.60	20.83
35	97.67	23.44
40	84.60	26.22

Table 2. C_s and L_{s_max} values for different D.

D/cm	C_s/nF	L_{s_max}/µH
15	146.11	30.00
20	171.32	30.00
25	210.83	30.00
30	276.26	30.00
35	386.29	30.00
40	671.40	30.00

3.4. The Flowchart of FTOE Method

A flowchart of the FTOE method is shown in Fig. 6 and described as follows:

(i) The system parameters, including the input impedance values, optimum load resistor values, C_s values and C_p values, are set. First, the input impedance values before matching and after matching are calculated when D is ranged from 15 cm to 40 cm in a step of 5 cm. Secondly, the optimum load resistor values are calculated when D is ranged from 15 cm to 40 cm in a step of 5 cm. Thirdly, C_s and C_p values are also calculated according to the optimum load resistors. Finally, all values are represented in the form of a matrix.

(ii) When switch S_1 is on ($S_1 = 1$), and switch S_2 is off ($S_2 = 0$), the extended L-type matching network is bypassed.

(iii) The input current and input voltage can be monitored by using current and voltage sensors;

(iv) The input impedance can be obtained by the input current and input voltage. We continuously collect 20 input impedance values. If the condition of $Z_{in}(20)$–$Z_{in}(1) < 0.01$ is satisfied, the input impedance is stable. $Z_{in}(20)$ is the twentieth input impedance. $Z_{in}(1)$ is the first input impedance.

(v) Comparing the current input impedance value with all input impedance values calculated in the first step, the minimum difference E_{bef} between the current input impedance and all input impedance values before matching can be found; the minimum difference E_{aft} between the current input impedance and all input impedance values after matching can be found. If the condition of $E_{bef} < E_{aft}$ is satisfied, the system operates at the state before matching. Conversely, the system operates at the state after matching.

(vi) When the system operates at the state before matching, if the current input impedance value is equal to the previous input impedance value, the transfer distance is not changed; if the current input impedance value is not equal to the previous input impedance value, the transfer distance is changed. Then the system restarts to match.
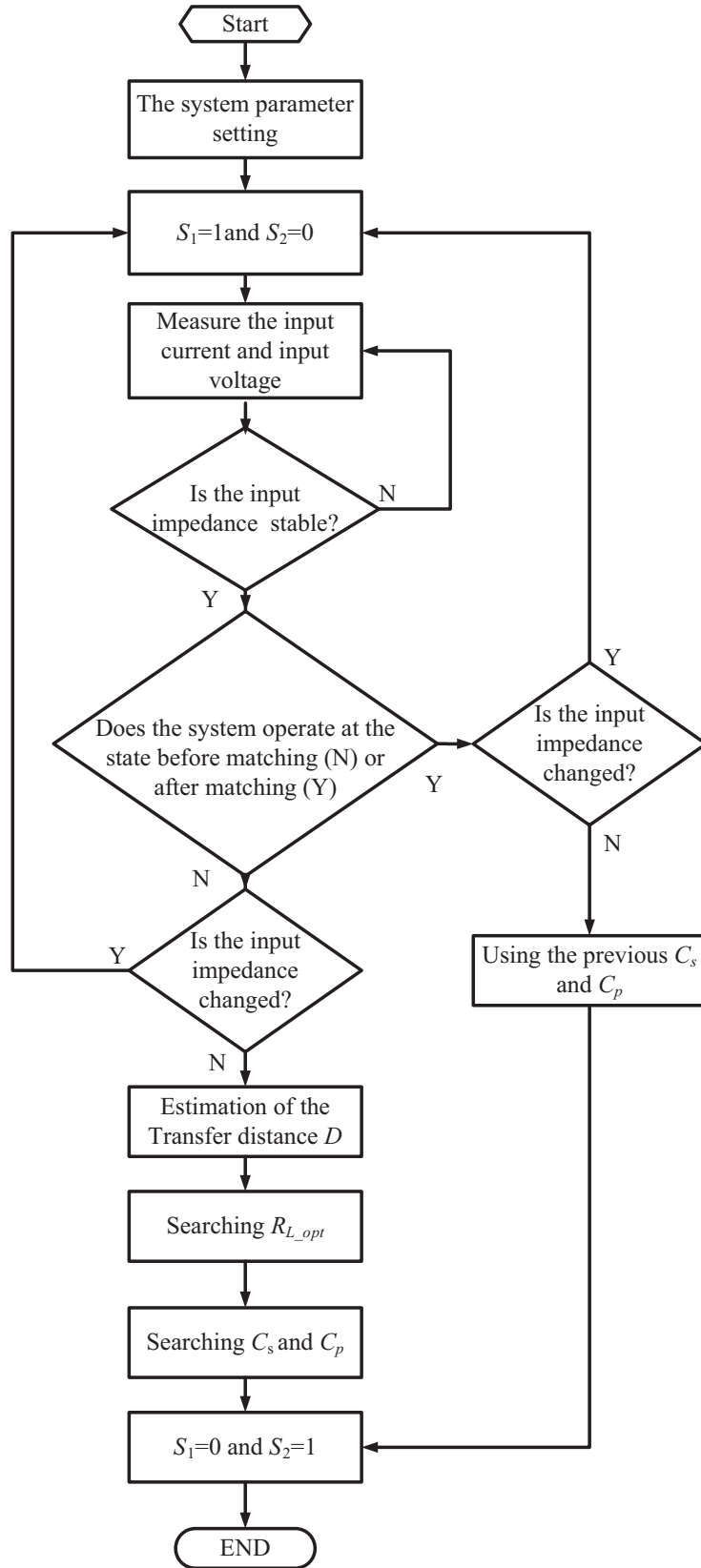
Figure 6. The flowchart of the FTOE method.

(vii) The transfer distance can be estimated according to the input impedance value.

(viii) The optimum load resistor can be found according to the transfer distance.

(ix) C_s and C_p values can be found according to the optimum load resistor.

(x) When switch S_1 is off ($S_1 = 0$), and switch S_2 is on ($S_2 = 1$), the L-type matching network is added into the system.

(xi) When the system operates at the state after matching, we can use the previous C_s and C_p values to match the system.

(xii) If the input impedance is changed, the system restarts to detect the input impedance.
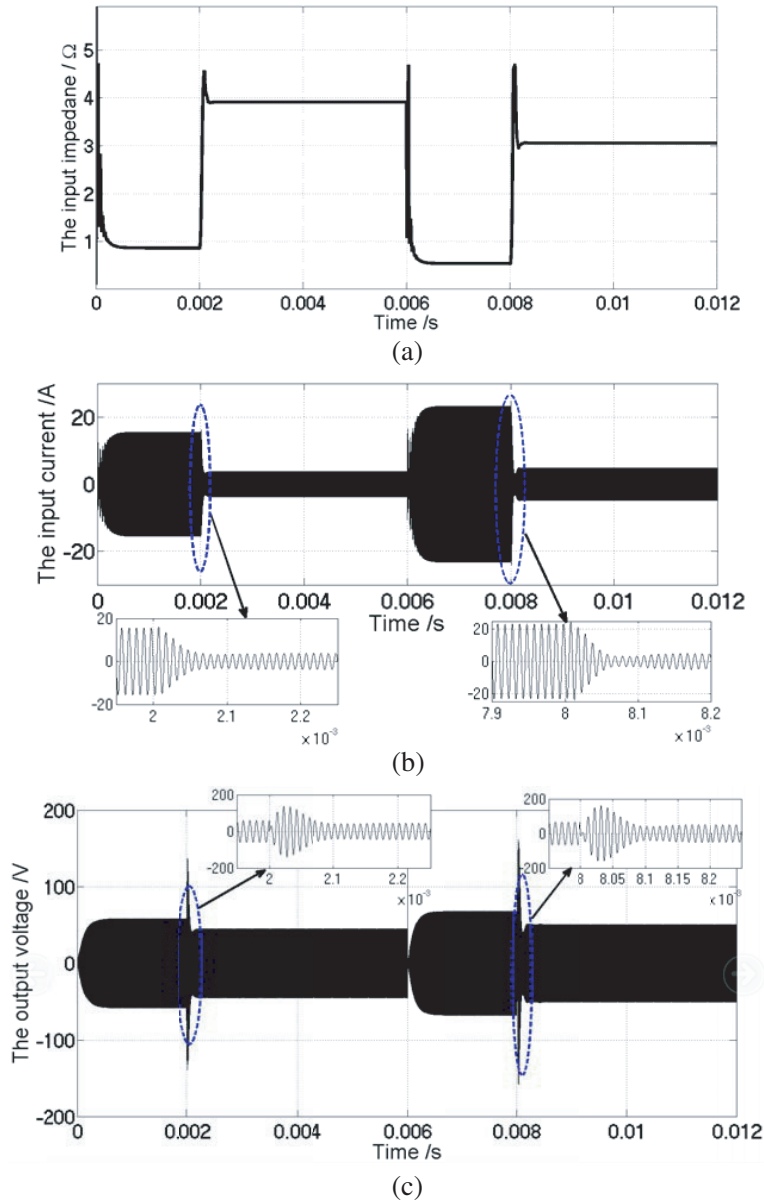
4. SIMULATION RESULTS

To validate the proposed method, the simulation model is built with the help of ANSYS Maxwell and MATLAB. The parameters of the system are shown in Table 3 in Section 5.
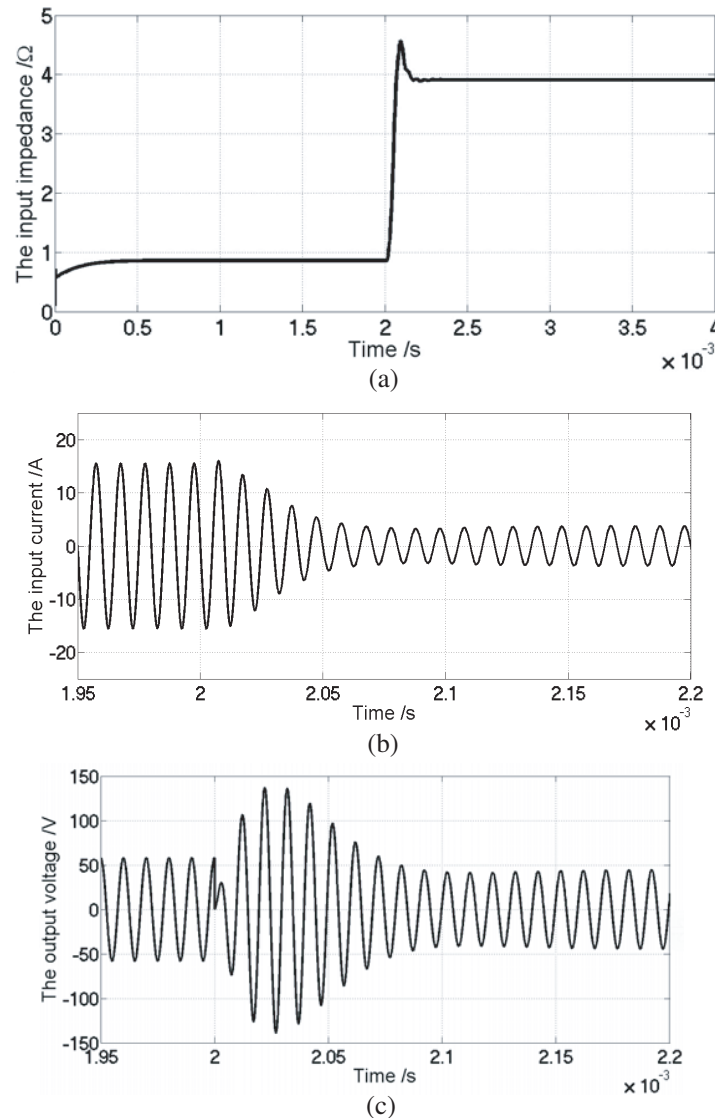
Figure 7. The simulation results with $D = 30$ cm. (a) The input impedance versus time. (b) The input current versus time. (c) The output versus time.

4.1. Fixed Transfer Distance

When the transfer distance is fixed at $30\,\mathrm{cm}$, the optimum load resistor can be obtained by the proposed method. In addition, the optimum input impedance can also be found. Fig. 7(a) shows the input impedance values. The system starts to automatically match at the time of $2\,\mathrm{ms}$. It can be seen that the input impedance value before matching is $0.86\,\Omega$, and the input impedance value after matching is $3.89\,\Omega$ from Fig. 7(a). Fig. 7(b) shows the input current values. It can be seen that the input current values before matching are larger than those after matching. The input current value before matching is $10.96\,\mathrm{A}$, whereas the input current value after matching is $2.62\,\mathrm{A}$. Fig. 7(c) shows the output voltage values. The output voltage value before matching is $41.1\,\mathrm{V}$, whereas the output voltage value after matching is $31.6\,\mathrm{V}$.

Figure 8. The simulation results with D changed from $30\,\mathrm{cm}$ to $25\,\mathrm{cm}$. (a) The input impedance versus time. (b) The input current versus time. (c) The output versus time.

4.2. Varied Transfer Distance

The transfer distance is initially set at 30 cm. Fig. 8(a) shows that the input impedance values versus time. It is clearly seen that the input impedance values are changed as the transfer distance is changed. The system starts to automatically match at the time of 2 ms with $D = 30$ cm. The input impedance value before matching is $0.86\,\Omega$, and the input impedance value after matching is $3.89\,\Omega$ with $D = 30$ cm. Then it is changed from 30 cm to 25 cm at the time of 6 ms. It can be seen that the input impedance value before matching is $0.54\,\Omega$, and the input impedance value after matching is $3.14\,\Omega$ with $D = 25$ cm.

Figure 8(b) shows the input current values versus time. It is clearly seen that the input current values after matching become smaller. The input current value before matching is 10.96 A, whereas the input current value after matching is 2.62 A with $D = 30$ cm. The input current value before matching is 16.48 A, whereas the input current value after matching is 3.29 A with $D = 25$ cm. Fig. 8(c) shows the output voltage values versus time. The output voltage value before matching is 41.1 V, whereas the output voltage value after matching is 31.6 V with $D = 30$ cm. The output voltage value before matching is 48 V, whereas the output voltage value after matching is 36 V with $D = 25$ cm.

The input power can be obtained by the input current multiplied by the input voltage. And the output power can be obtained by the output voltage (across the load resistor). The efficiency can be obtained by the output power divided by the input power. The efficiency before matching is 29%, and the efficiency after matching is 71% with $D = 30$ cm. The efficiency before matching is 26%, and the efficiency after matching is 74% with $D = 25$ cm. It is clearly seen that the optimum efficiency can be tracked by the proposed method.

5. EXPERIMENTAL VERIFICATION

To validate the proposed method, the prototype model of the system is built, as shown in Fig. 9. It is composed of a DC voltage source, four resonant coils, a full-bridge resonant inverter, a extended L-match network and the load. The transmitter on the left consists of a small S coil and a helical Tx resonant coil. The receiver on the right consists of a small L coil and a helical Rx resonant coil. The diameter of the Tx resonant coil is 40 cm with a pitch of 2 cm for approximately 6 turns. The parameters of the Rx coil are the same as those of the Tx coil. The S coil is a single loop and the diameter of the S coil is 50 cm, the parameters of the L coil are the same as those of the S coil. An impedance analyzer is used to extract the parameters in (1). The original resonant frequency is set to be 100 kHz. The parameters of the resonant coils are listed in Table 3.

Table 3. Parameters of the resonant coils.

Symbol	Quantity	Value
L_1	The inductance of S	1.86 μH
L_2	The inductance of Tx	29.70 μH
L_3	The inductance of Rx	29.70 μH
L_4	The inductance of L	1.90 μH
C_1	The external compensating capacitance of S	1.36 μF
C_2	The external compensating capacitance of Tx	85.28 nF
C_3	The external compensating capacitance of Rx	85.28 nF
C_4	The external compensating capacitance of L	1.33 μF
R_1	The resistor of S	0.07 Ω
R_2	The resistor of Tx	0.30 Ω
R_3	The resistor of Rx	0.29 Ω
R_4	The resistor of L	0.07 Ω
f_0	The original resonant frequency	100.0 kHz
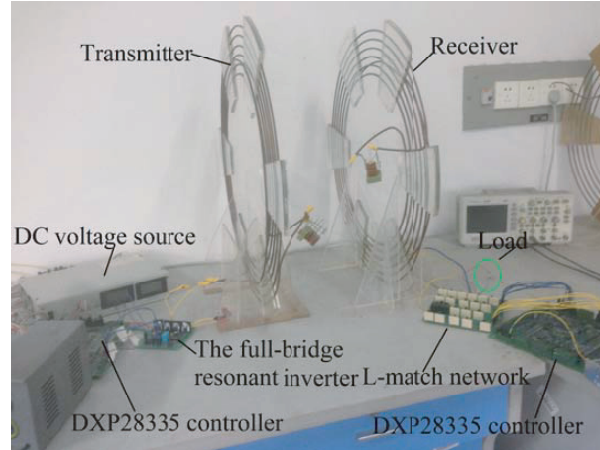
Figure 9. The experimental setup of the system.
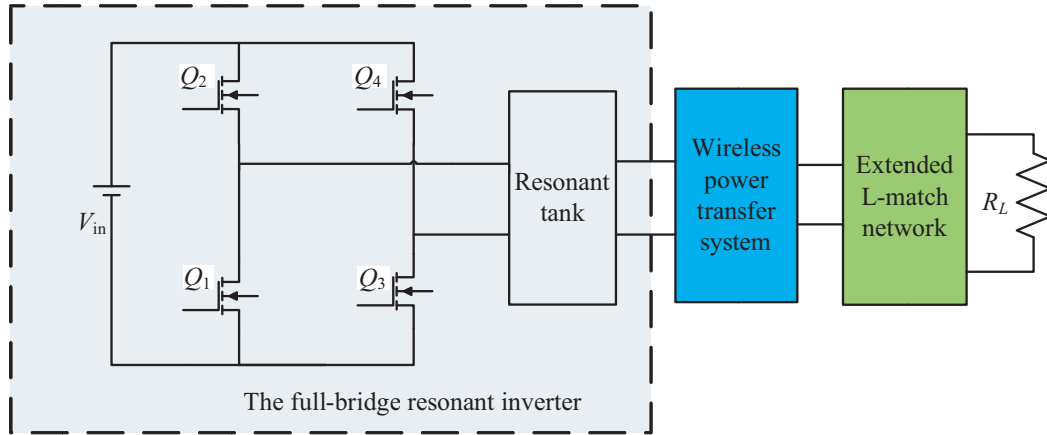
Figure 10. The schematic of the resonant inverter.

A full-bridge resonant inverter is used in this paper. Fig. 10 shows the schematic diagram of the inverter. The inverter consists of four switch MOSFETs ($Q_1 \sim Q_4$) and a resonant tank [21]. IR2110 and IRF3205 are used as the gate driver and switch MOSFET. The inverter is controlled by the pulse-width-modulation (PWM) signals from DXP28335 controller. An impedance network based on the capacitor matrix is implemented. A total of sixteen group capacitors are used in the capacitor matrix to realize different C_s and C_p configurations. DXP28335 controller periodically monitors the input current and calculates the input impedance. When the input impedance is changed, the controller decides to rematch the impedance network by adjusting C_s and C_p values. The high quality factor capacitors and the relay switches are used to realize the capacitor matrix.

The load resistor is fixed at $50\,\Omega$. We firstly test the reliability of the L-type matching network. L_s, C_s and C_p values are shown in Table 1 and Table 2 for different transfer distances. The equivalent load resistor values can be measured for different combinations of C_s and C_p. Fig. 11 shows R_{L_opt} versus the transfer distance D. It is clearly seen that R_{L_opt} is changed as D varies.

The input current can be collected by current sensors, and it can be observed in Code Composer Studio. Fig. 12 shows the measured input current with $D = 30\,\text{cm}$. Fig. 12(a) shows the measured input current before matching. Fig. 12(b) shows the measured input current after matching. The measured input current before matching is 10.94 A, whereas the measured input current after matching is 3.04 A.

Figure 13 shows the measured input current with $D = 25\,\text{cm}$. Fig. 13(a) shows the measured input current before matching. Fig. 13(b) shows the measured input current after matching. The measured
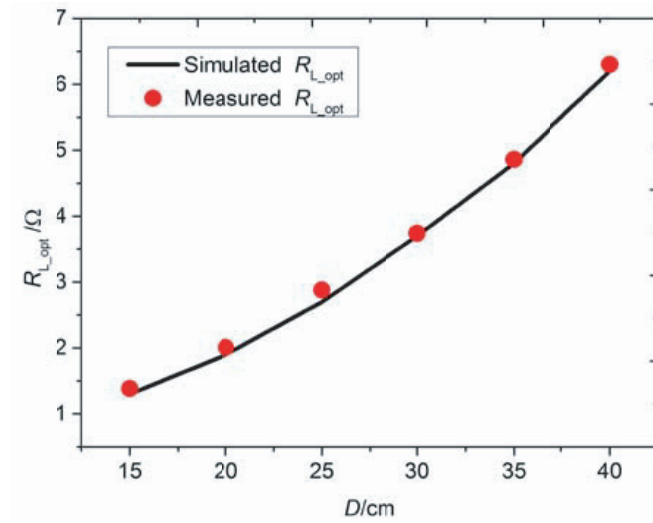
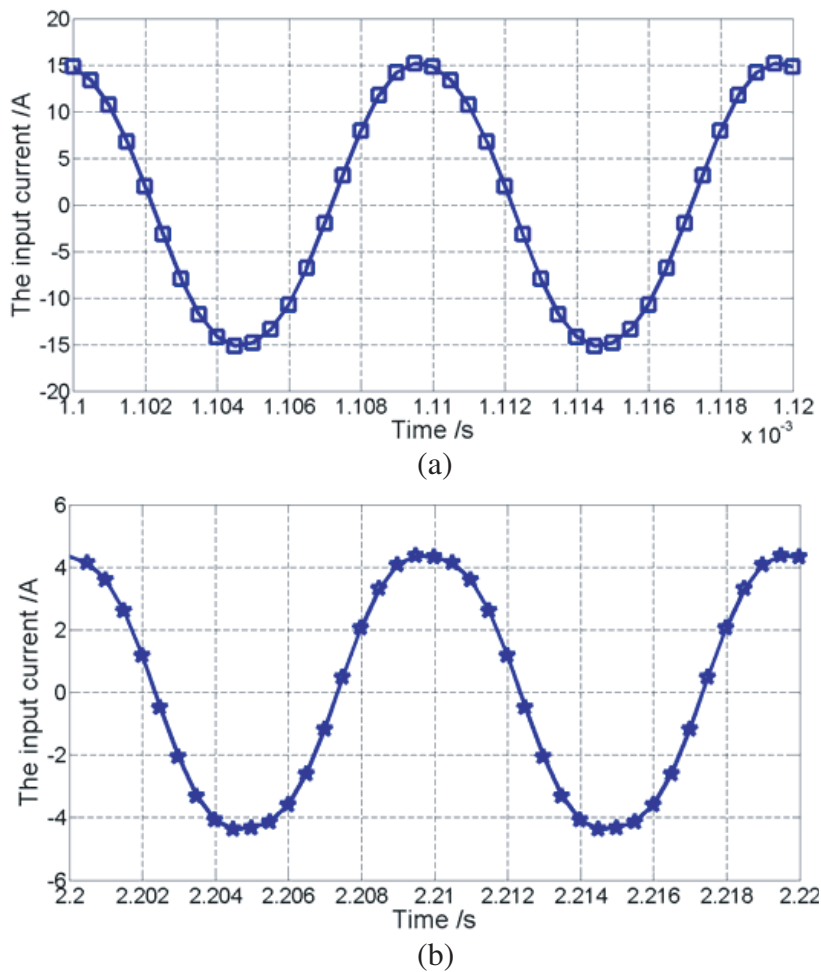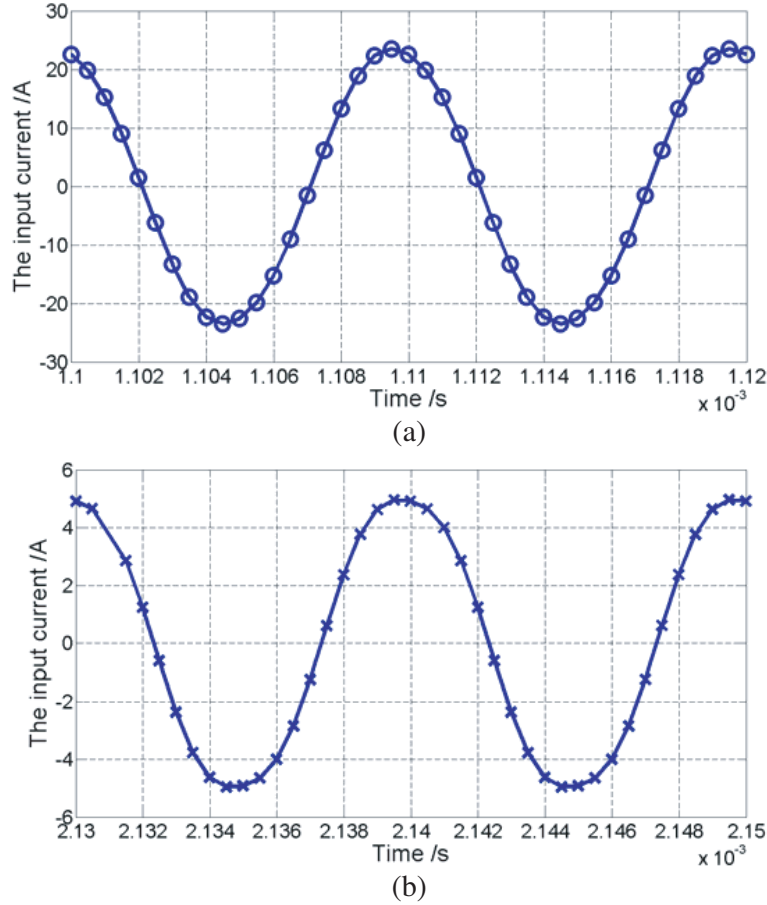**Figure 11.** R_{L_opt} versus D.

Figure 12. The input current versus time with $D = 30$ cm. (a) The input current before matching. (b) The input current after matching.

Figure 13. The input current versus time with $D = 25$ cm. (a) The input current before matching. (b) The input current after matching.

input current before matching is 16.60 A, whereas the measured input current after matching is 3.51 A. It is clearly seen that the measured input current before matching is larger than that after matching.

Figure 14 shows the calculated and measured Z_{in} before and after matching. It can be seen that Z_{in} before matching is smaller than that after matching. Z_{in} is changed as the transfer distance is ranged from 15 cm to 40 cm. Z_{in} before matching is ranged from $0.164\,\Omega$ to $0.309\,\Omega$, whereas Z_{in} after matching is ranged from $1.822\,\Omega$ to $6.085\,\Omega$.

Figure 15 shows the calculated and measured efficiencies before and after matching. When the impedance matching is not satisfied, the higher the efficiency is, the longer the transfer distance is. However, the maximum efficiency is 30.9% as the transfer distance is varied from 15 cm to 40 cm. When the impedance matching is satisfied, the higher the efficiency is, the shorter the transfer distance is. The maximum efficiency is 72.7% as the transfer distance is varied from 15 cm to 40 cm. The optimum efficiency can be tracked by the proposed method as the transfer distance is changed. It can be seen that the measured efficiency is 77.1%, whereas the simulated efficiency is only 72.7% with $D = 15$ cm. Although there is 5% power loss on the L-type matching network, the overall efficiency with the L-type matching network is still higher than that without the L-type matching network.

The number of the search steps using different methods can be obtained in [19]. The optimum number of the search steps is 42 when the method of the linear search is used; the optimum number of the search steps is 9 when the method of the binary search is used; the optimum number of the search steps is 6 when the method of the effective window prediction search is used. However, the optimum number of the search steps is 1 when the proposed method in this paper is used. This is because the transfer distance can be estimated and the optimum C_s and C_p can be obtained.
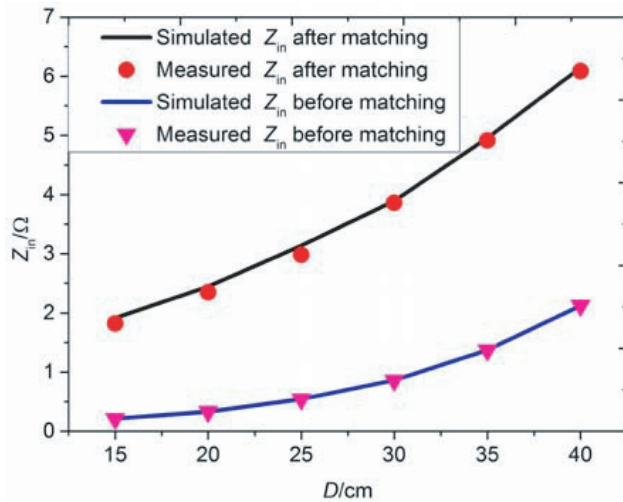
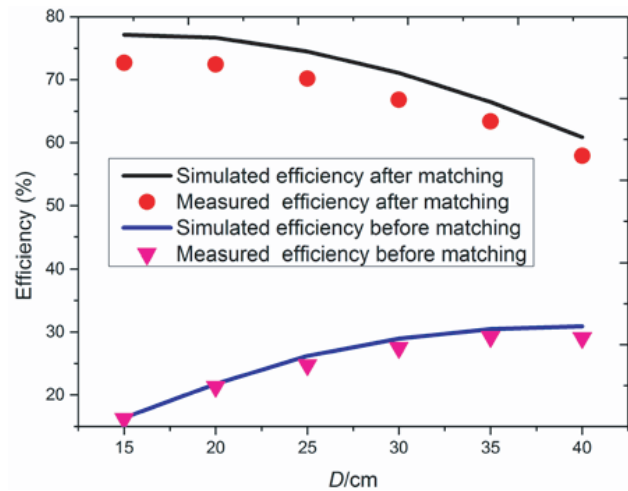**Figure 14.** The input impedance versus D.

Figure 15. Efficiency versus D.

6. CONCLUSIONS

In this paper, a fast tracking optimum efficiency method is presented. The extended L-type matching network is proposed in order to adjust the equivalent load resistor. The efficiency can be improved for different transfer distances by the proposed method. For example, the efficiency before matching is 27.5%, and the efficiency after matching is 66.8% with $D = 30$ cm. The optimum efficiency can be tracked automatically as the transfer distance is changed. The efficiency is changed from 66.8% to 70.2% when the transfer distance is changed from 30 cm to 25 cm. The advantage of the proposed method is that the system need not continuously search the optimum C_s and C_p because the transfer distance can be estimated. And the optimum C_s and C_p can be obtained according to R_{L_opt}. The number of switches is reduced. Therefore, the proposed method allows for an efficient and robust wireless power transfer system for charging of mobile.

ACKNOWLEDGMENT

REFERENCES

1. Kurs, A., A. Karalis, R. Moffatt, et al., "Wireless power transfer via strongly coupled magnetic resonances," *Science*, Vol. 317, No. 5834, 83–86, 2007.

2. Karalis, A. J. D. Joannopoulos, and M. Soljačić, "Efficient wireless non-radiative mid-range energy transfer," *Annals of Physics*, Vol. 323, No. 1, 34–48, 2008.

3. Kurs, A., R. Moffatt, and M. Soljacic, "Simultaneous mid-range power transfer to multiple devices," *Applied Physics Letters*, Vol. 96, No. 4, 044102–044102-3, 2010.

4. Chen, J., Z. Ding, and Z. Hu, "Metamaterial-based high-efficiency wireless power transfer system at 13.56 MHz for low power applications," *Progress In Electromagnetics Research B*, Vol. 72, No. 1, 17–30, 2017.

5. Shaw, T., A. Roy, and D. Mitra, "Efficiency enhancement of wireless power transfer system using MNZ metamaterials," *Progress In Electromagnetics Research C*, Vol. 68, No. 1, 11–19, 2016.

6. Shin, J., S. Shin, Y. Kim, et al., "Design and implementation of shaped magnetic-resonance-based wireless power transfer system for roadway-powered moving electric vehicles," *IEEE Transactions on Industrial Electronics*, Vol. 61, No. 3, 1179–1192, 2014.

7. Ram Rakhyani, A. K., S. Mirabbasi, and M. Chiao, "Design and optimization of resonance-based efficient wireless power delivery systems for biomedical implants," *IEEE Transactions on Biomedical Circuits and Systems*, Vol. 5, No. 1, 48–63, 2011.

8. Choi, S. Y., B. W. Gu, S. W. Lee, et al., "Generalized active EMF cancel methods for wireless electric vehicles," *IEEE Transactions on Power Electronics*, Vol. 29, No. 11, 5770–5783, 2014.

9. Wei, X. Z., Z. S. Wang, and H. F. Dai, "A critical review of wireless power transfer via strongly coupled magnetic resonances," *Energies*, Vol. 7, No. 7, 4316–4341, Jul. 2014.

10. Sample, A. P., D. A. Meyer, and J. R. Smith, "Analysis, experimental results, and range adaptation of magnetically coupled resonators for wireless power transfer," *IEEE Transactions on Industrial Electronics*, Vol. 58, No. 2, 544–554, 2011.

11. Kim, N. Y., K. Y. Kim, J. Choi, et al., "Adaptive frequency with power-level tracking system for efficient magnetic resonance wireless power transfer," *Electronics Letters*, Vol. 48, No. 8, 452–454, 2012.

12. Park, J., Y. Tak, Y. Kim, et al., "Investigation of adaptive matching methods for near-field wireless power transfer," *IEEE Transactions on Antennas and Propagation*, Vol. 59, No. 5, 1769–1773, 2011.

13. Duong, T. P. and J.-W. Lee, "Experimental results of high-efficiency resonant coupling wireless power transfer using a variable coupling method," *IEEE Microwave and Wireless Components Letters*, Vol. 21, No. 8, 442–444, 2011.

14. Huang, S., Z. Li, Y. Li, et al., "A comparative study between novel and conventional four-resonator coil structures in wireless power transfer," *IEEE Transactions on Magnetics*, Vol. 50, No. 11, 1–4, 2014.

15. Fu, M., C. Ma, and X. Zhu, "A cascaded boost-buck converter for high efficiency wireless power transfer systems," *IEEE Transactions on Industrial Informatics*, Vol. 10, No. 3, 1972–1980, 2014.

16. Liu, S., L. Chen, Y. Zhou, et al., "A general theory to analyse and design wireless power transfer based on impedance matching," *International Journal of Electronics*, Vol. 101, No. 10, 1375–1404, Oct. 2014.

17. Li, H., J. Li, K. Wang, et al., "A maximum efficiency point tracking control scheme for wireless power transfer systems using magnetic resonant coupling," *IEEE Transactions on Power Electronics*, Vol. 30, No. 7, 3998–4008, 2015.

18. Zhong, W. X. and S. Y. R. Hui, "Maximum energy efficiency tracking for wireless power transfer systems," *IEEE Transactions on Power Electronics*, Vol. 30, No. 7, 4025–4034, Jul. 2015.

19. Lim, Y., H. Tang, S. Lim, et al., "An adaptive impedance-matching network based on a novel capacitor matrix for wireless power transfer," *IEEE Transactions on Power Electronics*, Vol. 29, No. 8, 4403–4413, 2014.

20. Conway, J. T., "Inductance calculations for noncoaxial coils using bessel functions," *IEEE Transactions on Magnetics*, Vol. 43, No. 3, 1023–1034, 2007.

21. Ye, Z., P. K. Jain, and P. C. Sen, "A full-bridge resonant inverter with modified phase-shift modulation for high-frequency AC power distribution systems," *IEEE Transactions on Industrial Electronics*, Vol. 54, No. 5, 2831–2845, 2007.